Three-dimensional bioprinting of embryonic stem cells directs highly uniform embryoid body formation

2015 Biofabrication 7 044101

(http://iopscience.iop.org/1758-5090/7/4/044101)

Biofabrication

PAPER

Three-dimensional bioprinting of embryonic stem cells directs highly uniform embryoid body formation

Liliang Ouyang[1,2,6], **Rui Yao**[1,2,6], **Shuangshuang Mao**[1,2], **Xi Chen**[3], **Jie Na**[3] **and Wei Sun**[1,2,4,5]

[1] Biomanufacturing Center, Department of Mechanical Engineering, Tsinghua University, Beijing 100084, People's Republic of China
[2] Biomanufacturing and Rapid Forming Technology Key Laboratory of Beijing, Beijing 100084, People's Republic of China
[3] Center for Stem Cell Biology and Regenerative Medicine, School of Medicine, Tsinghua University, Beijing 100084, People's Republic of China
[4] Biomanufacturing Engineering Research Laboratory, Graduate School at Shenzhen, Tsinghua University, Shenzhen 518055, People's Republic of China
[5] Department of Mechanical Engineering, Drexel University, Philadelphia, Pennsylvania 19104, USA
[6] These authors contributed to this work equally

E-mail: weisun@tsinghua.edu.cn **and** sunwei@drexel.edu

RECEIVED
16 April 2015

REVISED
19 June 2015

ACCEPTED FOR PUBLICATION
26 June 2015

PUBLISHED
4 November 2015

Keywords: embryonic stem cell, 3D bioprinting, embryoid body formation

Supplementary material for this article is available online

Abstract

With the ability to manipulate cells temporarily and spatially into three-dimensional (3D) tissue-like construct, 3D bioprinting technology was used in many studies to facilitate the recreation of complex cell niche and/or to better understand the regulation of stem cell proliferation and differentiation by cellular microenvironment factors. Embryonic stem cells (ESCs) have the capacity to differentiate into any specialized cell type of the animal body, generally via the formation of embryoid body (EB), which mimics the early stages of embryogenesis. In this study, extrusion-based 3D bioprinting technology was utilized for biofabricating ESCs into 3D cell-laden construct. The influence of 3D printing parameters on ESC viability, proliferation, maintenance of pluripotency and the rule of EB formation was systematically studied in this work. Results demonstrated that ESCs were successfully printed with hydrogel into 3D macroporous construct. Upon process optimization, about 90% ESCs remained alive after the process of bioprinting and cell-laden construct formation. ESCs continued proliferating into spheroid EBs in the hydrogel construct, while retaining the protein expression and gene expression of pluripotent markers, like octamer binding transcription factor 4, stage specific embryonic antigen 1 and Nanog. In this novel technology, EBs were formed through cell proliferation instead of aggregation, and the quantity of EBs was tuned by the initial cell density in the 3D bioprinting process. This study introduces the 3D bioprinting of ESCs into a 3D cell-laden hydrogel construct for the first time and showed the production of uniform, pluripotent, high-throughput and size-controllable EBs, which indicated strong potential in ESC large scale expansion, stem cell regulation and fabrication of tissue-like structure and drug screening studies.

1. Introduction

With the capability of self-renewal and differentiating into all somatic cell types, embryonic stem cells (ESCs) hold great promise as an *in vitro* model system for studies in early embryonic development, as well as a robust cell source for applications in diagnostics, therapeutics, and drug screening [1]. Derived from the inner cell mass of a blastocyst, ESCs requires delicate culture condition and trend to cluster together, and in particular, forms three-dimensional (3D) cellular spheroids termed embryoid body (EB) [2]. In order to better understand stem cell niche and regulation of ESC differentiation and reprogramming, *in vitro* recapitulation of the spatial distribution of cells, cell–cell and cell–matrix interactions, is of paramount importance [3–5]. Compared with 2D monolayer culture, 3D cell culture is believed to confer a higher degree of clinical and biological relevance to *in vitro* model [6, 7], since the spatial arrangement of cells and extra-

cellular matrix could influence cell differentiation and function both *in vivo* [8] and *in vitro* [9]. Therefore, reconstruction of 3D cell microenvironment is critical to directing stem cell fate and generating cell sources for tissue engineering, regenerative medicine and drug screening studies.

By mimicking some of the spatial and temporal aspects of *in vivo* development, EB is a basic 3D model for ESCs culture and differentiation studies. It was reported that the size and uniformity of EBs could vastly influence stem cell fate [10–12]. Various methods have been used to fabricate such cellular spheroid, basically including static suspension, hanging-drop and multiwell culture, most of which doesn't involve biomaterials. Static suspension method inoculate suspension of ESCs onto non-adhesive plate to allow cells spontaneously aggregate into spheroid. This method is easy to operate, but showed limited control over the EBs size and shape due to the probability that ESCs encounter each other accidentally [13]. Hanging-drop is a common method to produce size-controlled homogeneous EBs, where droplets of ESCs suspension are pipetted onto the lid of a Petri dish and EBs was generate by gravity after overturning the dish [14]. However, manual pipetting is labor intensive and the reproducibility varies with operators. Multiwell culture offers high-throughput solution for EB formation through cell aggregation in uniformly shaped microwell arrays but requires expensive microwell culture plates [10, 15]. Besides, there are few customized microwell culture plates available in the market.

Recent advances in bioprinting technologies facilitated the precise deposition of ESCs in a reproducible manner. Xu *et al* [16] and Shu *et al* [17] printed ESCs suspension solution into 2D patterns as hanging-drop approach for EB formation, without the cell-biomaterial interaction. Corr and Xie [18, 19] applied laser direct-write method in bioprinting of mouse ESCs together with gelatin. ESCs maintained the pluripotency while proliferation and formed EB. EB size can be controlled by cell density and colony size. However, these studies just generated 2D cellular array without 3D cell–matrix interactions, and cell–cell interaction happens within one drop but not among different drops. To better recapitulate the characteristics of *in vivo* cell microenvironment, 3D customized cell/matrix construct with macro-porous structure might be a preferred choice. To our knowledge, there has been no report about bioprinting of ESCs into 3D cell-laden constructs.

The extrusion-based temperature-sensitive 3D bioprinting technology was developed in our lab and has been utilized for bioprinting of hepatocytes [20], adipose tissue-derived stem cells (ADSCs) [21], C2C12 cells [22], hela cells [23] and 293FT cells [24]. Most commonly used biomaterials for this technology are gelatin and alginate. Gelatin, a type of denatured collagen, is widely used as a coating for feeder layer-free mouse ES cell culture. Alginate, extracted from brown algae, is proving to have a wide applicability in tissue engineering and drug delivery and also used in embedding mouse ESCs for EB formation [25]. It has been proved in many studies that encapsulation of ESCs in hydrogels would direct EB formation with the maintenance of pluripotency [26–28]. Hence, we hypothesized that the bioprinting of 3D ESC-laden construct would maintain the stem cell pluripotency and address the challenges associated with the current methods for EB formation.

In this study, we investigated the feasibility of applying extrusion-based temperature-sensitive 3D bioprinting technology in bioprinting of ESCs with hydrogels into 3D macro-porous structure, with the maintenance of viability, pluripotency, cell growth and to direct EB formation. Printing process parameters were optimized to obtain a high cell survival rate (90%) after printing process and construct formation. Stem cell pluripotency was examined by the expression of stem cell markers (octamer binding transcription factor 4 (Oct4), stage specific embryonic antigen 1 (SSEA1) and a homeodomain-bearing transcriptional factor (Nanog)) and the ability to form EBs. The regulation of EB formation in the 3D bioprinted construct was systematically compared with commonly used methodology, where EB formation relies on cell aggregating as well as cell proliferation. Results demonstrated that this novel technology generated pluripotent, high-throughput, highly uniform and size controllable EBs under static culture condition without complex equipment. This study established the feasibility of fabricating 3D *in vitro* tissue-like model using ESCs for the first time, creating engineered microenvironment for pluripotent stem cells with the ability of placing cells and materials spatially in a reproducible manner.

2. Materials and methods

2.1. Materials preparation

Gelatin (Sigma-Aldrich, G1890) and sodium alginate (Sigma-Aldrich, A0682) were dissolved in 0.5% (w/v) sodium chloride solution at the concentration of 15% (w/v) and 4% (w/v), respectively. Both the two solutions were sterilized under 70 °C for 30 min for three times with the interval time of 30 min. The sterilized solutions were packed into 1.5 mL EP tubes, stored at 4 °C and incubated at 37 °C before use.

2.2. ES cell culture

Undifferentiated mES cell line (R1, obtained from NaJie lab, Center for Stem Cell Biology and Regenerative Medicine, Tsinghua University, China) were cultured in DMEM (Gibco, 11960-044) supplemented with 15% knock out TM SR serum replacement for ESC/iPSCs (Gibco, 10828-028), 0.1 mM MEM non-essential amino acids (Gibco, 11140-050), 2 mM GlutaMax-1 (Gibco, 35050-061), 1 mM sodium

pyruvate (Gibco, 11360-070), 100 U mL^{-1} penicillin/streptomycin (Gibco, 10378-016), 1000 U mL^{-1} leukemia inhibitory factor (LIF: ESGRO, ESG1106) and 0.1 mM β-mercaptoethanol. Cells were passaged every 2 to 3 days with 0.025% trypsin/ethylene diamin tetraacetate (EDTA) onto 0.1% gelatin-coated Petri dish.

2.3. Bioprinting and culture of 3D ESC-laden hydrogel construct

ESCs were bioprinted with matrix materials using an extrusion-based 3D bioprinter following the previously established methods [24]. Briefly, 600 μL of gelatin solution and 400 μL of alginate solution was warmed under 37 °C for 20 min, gently mixed as matrix material and used within 30 min ESCs was collected, dispersed into single cells and 200 μL cell suspension was gently mixed with matrix material under room temperature with the cell density of 0.5, 1.0 and 2.0 million mL^{-1}, respectively. 30 mm Petri dishes were coated with 0.0125% (w/v) poly-L-Lysine (Sigma-Aldrich, P8920) and used as collecting plate in the 3D bioprinting process. Within a temperature-controlled chamber of the 3D bioprinter, whose temperature was set within the gelation region of gelatin, the mixture of ESCs and matrix materials was bioprinted into a cubic construct layer by layer in a zigzag fashion. The nozzle insulation temperature and printing chamber temperature were set at 25 °C/30 °C and 4 °C/7 °C/10 °C, respectively, while nozzles with inner diameter of 160 μm/260 μm/410 μm/510 μm were chose for printing. The dimensions of the cubic construct was 8 mm × 8 mm, with six layers in height. After the temperature controlled bioprinting process, the printed 3D constructs were immersed in 100 mM calcium chloride for 3 min for crosslinking, and then washed with phosphate buffer solution (PBS) for three times. The whole printing process was finished in 30 min. The 3D crosslinked construct was cultured by ESC culture medium in the atmosphere of 5% CO_2 at 37 °C. Culture medium was refreshed every 1 to 2 days. The cell morphology was examined and recorded by an optical microscope (Olympus, CX40).

2.4. Suspension and hanging-drop for EB formation

Suspension cultures of EBs were initiated by resuspending ESCs in culture medium, and cultivated in sterile 30 mm Petri dishes coated with 2% agar (generating a low-adherence surface for suspension culture) with final cell amount of 0.5 million in 1.5 mL culture medium. Hanging-drop EBs were prepared by suspending 10^4 cells/mL in culture medium in 20 μL drops on the lid of a 100 mm Petri dish. Then the lid was carefully inverted and put over the bottom of the dish filled with PBS to prevent the drops from drying out. EBs formed using these two methods were cultured for 96 h and the EBs phase images were captured by an optical microscope (Olympus, CX40) every day.

2.5. Live/dead assay

A fluorescent live/dead staining was used to determine cell viability in the 3D cell-laden constructs according to the manufacturer's instructions. Briefly, samples were gently washed in PBS for 3 times. 1 μM Calcein-AM (Sigma-Aldrich, 17783) and 2 μM propidium iodide (Sigma-Aldrich, P4170) were used to stain live cells (green) and dead cells (red) for 15 min while avoiding light. A laser scanning confocal microcopy system (LSCM, Nikon, Z2) was used for image acquisition. Cell viability was counted by count/size tool of Image-Pro-Plus and calculated by dividing the total number of cells by green stained cells. Three random fields were counted for each sample.

2.6. EB harvest

To harvest the EBs in the construct, the 3D constructs were dissolved by adding 55 mM sodium citrate and 20 mM EDTA in 150 mM sodium chloride [29] for 5 min, while gently shake the Petri dish for better dissolving. After being transferred to 1.5 mL EP tubes, the EB suspensions were centrifuged under 200 rpm for 3 min, and the supernatant liquid was removed to harvest EBs for further analysis.

2.7. Cell proliferation analysis

Cell counting kit-8 (Dojindo, CCK-8) was used to determine the proliferation of ESCs in monolayer culture (2D) and printed construct (3D) as previously stated [24]. 3D construct samples were divided into two treatment groups: with ESCs embedded in the 3D hydrogel construct (labeled as '*in situ*'), and with ESCs harvested from the construct (labeled as 'harvest'). Both 2D and 3D samples were incubated with 80 μL CCK-8 solution in 800 μL culture medium for 2 h at 37 °C. Then 110 μL supernatant were transferred to one well of 96-well plate in a microplate reader (BIO-RAD, Model 680) to read optical density (OD) at 450 nm wavelength. EB volume, which was determined by the function $V = \pi d^3/6$ (V means EB volume, d means EB diameter), was also used to assess cell growth in 3D constructs. OD value from CCK-8 and EB volume were normalized to the data of day 1 through dividing data of day 1 by that of each day for comparison. Three samples were tested for each group.

2.8. EB morphology analysis

To assess the EB morphology, the collected EBs were resuspended in 500 μL PBS. Afterwards the EB suspension were transferred to a 35 mm Petri dish. The dish was gently shaken so that EBs distributed evenly on the bottom. To capture the micro-images of EBs, an optical imaging system (Olympus CK40) was used. EB diameter and circularity were measured to characterize the EB morphology. EB diameter (D) is defined by the equation $D = (4A/\pi)^{1/2}$, where A means the area of EB cross-section. EB circularity (C)

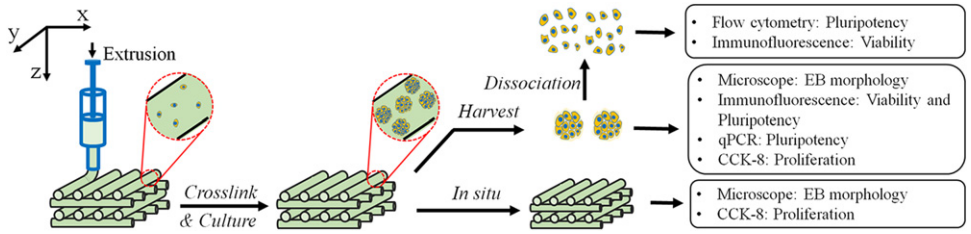

Figure 1. Schematic representation of this research.

is determined by the equation $C = 4\pi A/L^2$, where L means the perimeter of EB cross-section. To calculate the geometrical parameters like A and L, the geometrical outline of EB cross-section was extracted using an image recognition program in Matlab (supplement 1). 250 EBs were used for data statistics for each process parameters configuration. In addition, this program was also used in the semi-quantitative analysis for calculating area occupied by EB in the construct through dividing the area of grid hydrogel structure by the area of all EBs.

2.9. Immunohistochemical analysis

To examine the pluripotency of EBs in the 3D construct, EBs were harvested, fixed with 4% paraformaldehyde for 20 min and permeabilized with 0.1% Triton-X 100 in PBST (0.1% Tween in PBS) for 30 min. After blocking with 5% bovine serum albumin (BSA) in PBST for 1 h, the EBs were incubated with the primary antibodies Oct4 (abcam, ab19857) and SSEA1 (abcam, ab16285) for 12 h at 4 °C. The EBs were washed with PBST and then incubated with the second antibodies Alexa Fluor® 594 (abcam, ab150080) and Alexa Fluor® 488 (abcam, ab150113) for 2 h. The controls were performed by replacing the primary antibodies with corresponding immunoglobulin G antibodies. The EBs were then washed with PBST and stained with DAPI. All images were analyzed using Nikon Z2 confocal microscope.

2.10. Flow cytometry analysis

Collected EBs were washed twice with PBS for 3 min at room temperature followed by StemPro® Accutase (Cell dissociation reagent, Life technologies, A11105-01) treatment for 5 min at 37 °C to dissociate EB to single cells. After centrifugation with 1000 rpm for 3 min, the cells were fixed, permeabilized and blocked as stated above. Then, the cells were incubated with the primary and second antibodies to mark Oct4 and SSEA1 separately, according to the manufacturer's instruction. The controls were performed by replacing the primary antibodies with PBS. After resuspension in sorting buffer (0.1% BSA in PBS), the cells were analyzed using a flow cytometer (FACSAria III, BD Biosciences).

2.11. RNA isolation and quantitative real time polymerase chain reaction (qRT-PCR)

After washing by PBS for three times, 1 mL Trizol (Invitrogen) was added to each sample, followed by a 10 min incubation one ice and 1 min stirring to complete homogenization. The mixtures were then transferred to 1.5 mL EP tube, supplemented with 200 μL chloroform followed by vigorous shaking and 5 min incubation at room temperature. Samples were then centrifuged at 12 000 rpm and 4 °C for 15 min and upper aqueous layer was collected to a new tube. RNA was isolated through being blended with isopropanol and followed by 15 min incubation at room temperature. After centrifuging at 12 000 rpm and 4 °C for 10 min, the supernatant was removed and the RNA was washed with 75% ethanol. After centrifuging at 7500 rpm and 4 °C for 5 min, the collected RNA was dissolved in DEPC water. The concentration of RNA was determined by measuring the absorbance at 260 nm in a spectrophotometer (Thermo Scientific) and the purity of RNA was estimated from the ratio of readings at 260 nm and 280 nm.

RNA samples were transcribed to cDNA using PrimeScript™ II 1st strand cDNA Synthesis Kit (TaKaRa). qRT-PCR was performed on a real time PCR detection system (CFX96, Bio-Rad) with Maxima SYBR Green qPCR master mix (Thermo Scientific) in triplicate as per manufacturer's instructions. Relative expression was determined by delta-delta Ct method with the expression of GADPH as housekeeping reference. The sequence of the gene specific primers for PCR were as follows: GAPDH, (5′ primer) CATCACCATCTTCCAGGAGC and (3′ primer) ATGCCAGTAGCTTCCCGTC; Oct4, (5′ primer) GAAGCAGAAGAGGATCACCTTG and (3′ primer) TTCTTAAGGCTGAGCTGCAAG; Nanog, (5′ primer) CCTCAGCCTCCAGCAGATGC and (3′ primer) CCGCTTGCACTTCACCCTTTG. Schematic representation of this research was demonstrated in figure 1.

2.12. Statistical analysis

All results were presented as the mean ± standard deviation. Statistical analysis was performed using two-way analysis of variance in conjugation with a Bonferroni post-hoc test and a student t-test in Graphpad Prism. Statistical significance was defined as

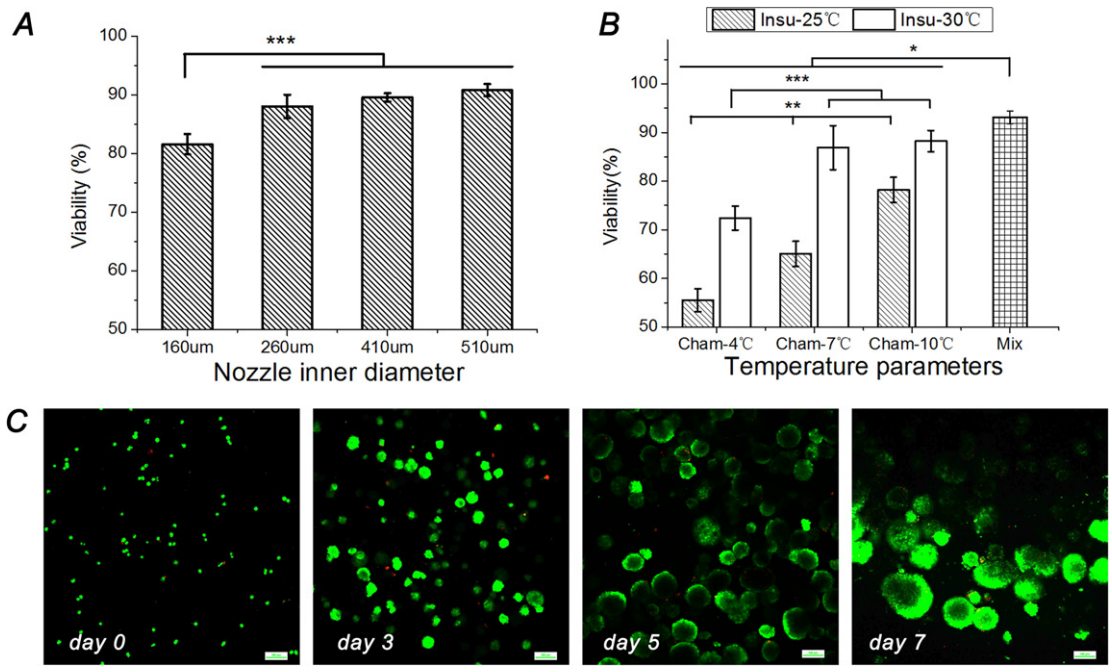

Figure 2. The influence of bioprinting parameters on ESC viability is determined by fluorescence live/dead staining. (A) The influence of printing nozzle inner diameter on ESC viability (Insu-30 °C and Cham-10 °C). (B) The influence of nozzle insulation temperature and chamber temperature on ESC viability. Insu-25 °C means keeping the nozzle insulation temperature at 25 °C. Cham-4 °C means setting the chamber temperature at 4 °C, and so as others. (C) The fluorescent staining images show the live (green) and dead (red) cells at different days during culture period. Scale bar: 100 μm.

$^{*}p < 0.05$, $^{**}p < 0.01$, and $^{***}p < 0.001$. Three independent trials were carried out unless otherwise stated.

3. Results

3.1. 3D bioprinting and cell viability optimization

In this study, many process parameters, e.g. nozzle inner diameter, nozzle insulation temperature and chamber temperature were examined to optimize cell viability after 3D construct fabrication. It was demonstrated that larger nozzle diameter resulted in higher cell viability (figure 2(A)). Specially, the cell viability under Nozzle-160 μm (81.59% ± 1.74%) was lower than those under Nozzle-260 μm (88.06% ± 1.98%), Nozzle-410 μm (89.59% ± 0.71%) and Nozzle-510 μm (90.84% ± 1.02%), with significant differences. Nozzle diameter of 260 μm, 410 μm and 510 μm showed no significant differences in terms of cell viability.

Insulation and chamber temperatures were altered to study their influences on cell viability (figure 2(B)). As a positive control, ESCs/hydrogel mixture without bioprinting were stained with fluorescence live/dead reagent, and showed 93.14% ± 1.31% cell viability. When insulation temperature was set at 25 °C (labeled as 'Insu-25 °C'), cell viability increased with the chamber temperature from 55.52% ± 2.37% under 4 °C (labeled as 'Cham-4 °C') to 78.22% ± 2.55% under 10 °C (labeled as 'Cham-10 °C') with significant differences. When the insulation temperature was set at 30 °C (labeled as 'Insu-30 °C'), nearly 90% ESCs remained alive under the chamber temperature of 7 °C and 10 °C (labeled as 'Cham-7 °C' and 'Cham-10 °C'), significantly more than that under Cham-4 °C (72.40% ± 2.46%). To achieve both high ESC viability and a clear construct configuration, the process parameter combination of Nozzle-260 μm, Cham-10 °C and Insu-30 °C was chosen.

After culturing for three days, few cells were found dead, which were isolated from living EBs (figure 2(C)). On day 5 and day 7, a few dead cells were observed on the edge of EBs. About 5% ESCs were stained dead on day 7. As the static culturing continued, 9.69% ± 1.77%, 17.72% ± 2.91% and 40.64% ± 2.06% were found dead on day 8, day 9 and day 10, respectively (supplement 2). So, we chose 7 days as the culture period in the following analysis.

3.2. Construct structural stability and EB formation

A 3D cellular construct with the cross section of 8 mm × 8 mm and height of 1 mm was fabricated under the optimized process parameter. The 3D construct demonstrated macro-porous grid structure in which the hydrogel threads were evenly distributed according to the computer design (figure 3(A)). Both the width of the threads and the gap between the threads were homogeneous, that is 728.2 μm ± 24.9 μm and 424.3 μm ± 17.8 μm, respectively, suggesting 3D cellular construct formation in a highly controlled manner. ESCs were embedded uniformly in the hydrogel matrix threads, developing a specific 3D microenvironment.

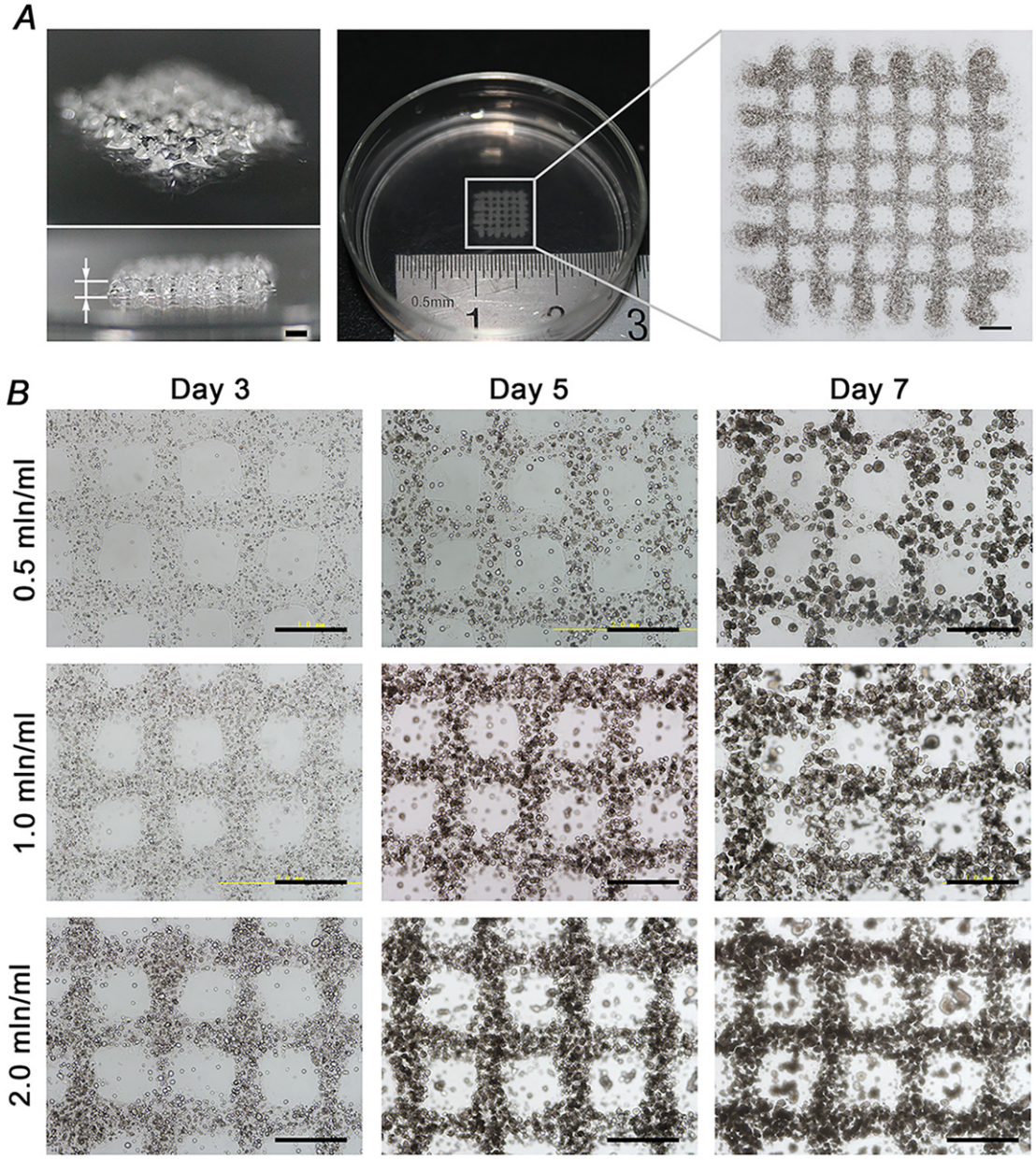

Figure 3. Images of the printed cellular model with grid structure. (A) Full view of the cellular construct. (B) Phase-contrast images demonstrating the cell morphology and distribution of different cell density at day 3, day 5 and day 7. Scale bar: 1 mm.

During the culture period, ESCs tended to grow as spheroid cellular aggregates, also known as EB. The cell density in the 3D hydrogel construct were determined by the initial cell density in the ESC/alginate/gelatin mixture and showed significant influence on the yield and density of EBs formed in the construct (figure 3(B)). It was demonstrated by semi-quantitative analysis of figure 3(B) that, the percentage of area occupied by EBs varied from 52% to 85% when initial cell density changed from 0.5 mln mL^{-1} to 2.0 mln mL^{-1}. Most of the EBs were contained in the hydrogel threads in the culturing period. However, when the initial cell density was as high as 2.0 mln ml^{-1}, some of the EBs were observed running off from the threads into the throughout holes.

3.3. Cell proliferation

ESCs formed spheroid EBs in the 3D hydrogel construct and the diameter of the EBs enlarged with culturing time while keeping their spatial location in the hydrogel thread, indicating EB formation by ESC proliferation rather than aggregation (figure 4(A)). Compared with traditional 2D culture, ESCs showed different proliferation rate indicated by the OD value measure by CCK-8 kit (figure 4(B)). The normalized OD value of the 3D *in situ* group grew faster than that of 2D from day 1 to day 3, while slowing down after day 3 and being much less than that of 2D at day 7. However, 3D harvest group showed a generally faster growth rate than 2D during the one week culturing, with a significant difference. In addition, the diameter

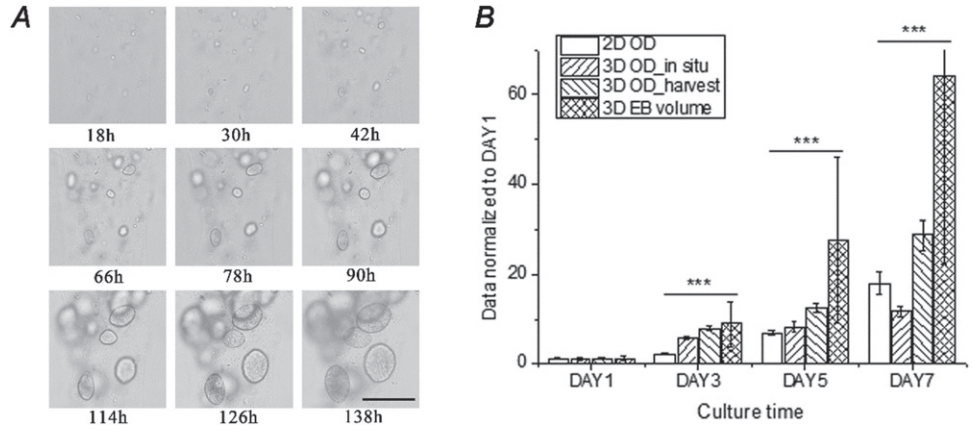

Figure 4. EB growing and cell proliferation. (A) Magnified images of the same location in 3D printed cellular construct at different times. (B) ESC proliferation in the 3D construct compared with 2D culture. All the date were normalized to the value of day 1. Scale bar: 200 μm.

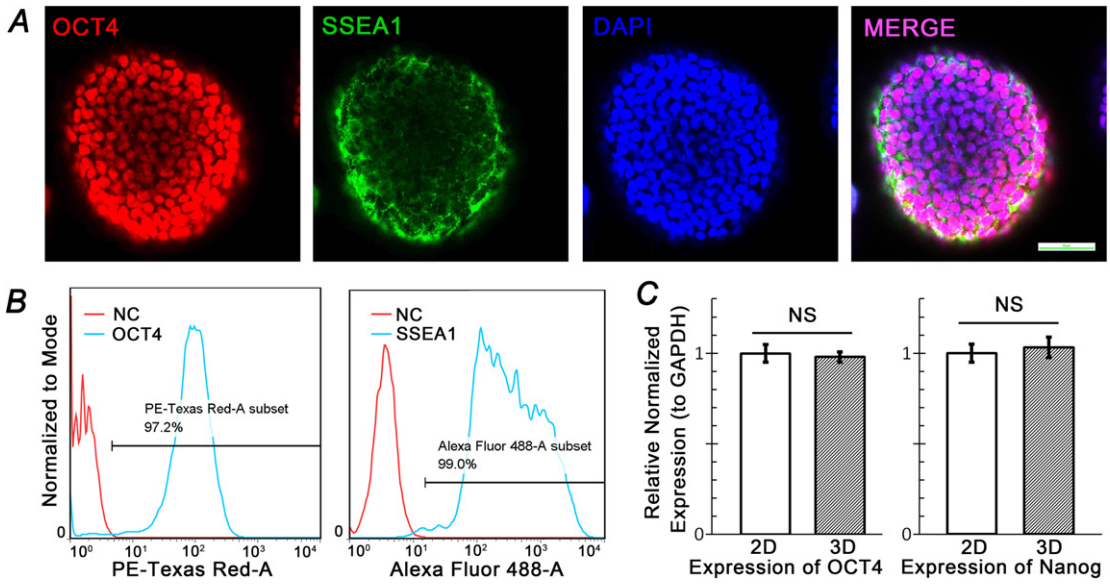

Figure 5. ESC pluripotency at day 7 was determined by CLSM, flow cytometry and qRT-PCR. (A) Immunofluorescence images of EBs stained with Oct4, SSEA1 and DAPI. (B) Quantification of 3D dissociated cells marked with Oct4 and SSEA1 by using flow cytometry. (C) Gene expression of Oct4 and Nanog in 3D versus 2D by using qRT-PCR. Scale bar: 50 μm.

of EB was also measured to indicate ESC proliferation rate. When comparing the normalized EB volume with normalized 2D OD value, 3D samples also maintained a significantly faster growth rate than 2D, though the EB volume had huge variance (figure 4(B)).

3.4. ESCs pluripotency maintenance

Pluripotency markers, i.e. Oct4, SSEA1 and Nanog were analyzed to determine the pluripotency maintenance of ESCs after 7 day culture in the 3D hydrogel construct. Immunofluorescence staining and flow cytometry analysis showed that almost all of the cells within the EB were successfully stained both Oct4 and SSEA1. Because of the limitation of confocal capacity when dealing with large scale aggregates, the central part of the EB was darker than the edge (figure 5(A)). Flow cytometry analysis demonstrated that 97.2% and 99.0% cells were positively stained with Oct4 and SSEA1 respectively (figure 5(B)). The qRT-PCR results demonstrated that the gene expression level of Oct4 and Nanog in our 3D samples were close to those in 2D (within the deviation of $\pm$3%), without significant difference, confirming that cells have maintained pluripotency (figure 5(C)).

3.5. EB morphology

EBs were harvested from the 3D hydrogel construct at different time intervals to analyze EB morphology (figure 6(A)). Most of the EBs were separated without fusion. The center part of the EBs was darker than edge part, especially at day 5 and day 7, indicating the 3D sphere structure of EBs. Through analyzing the size of

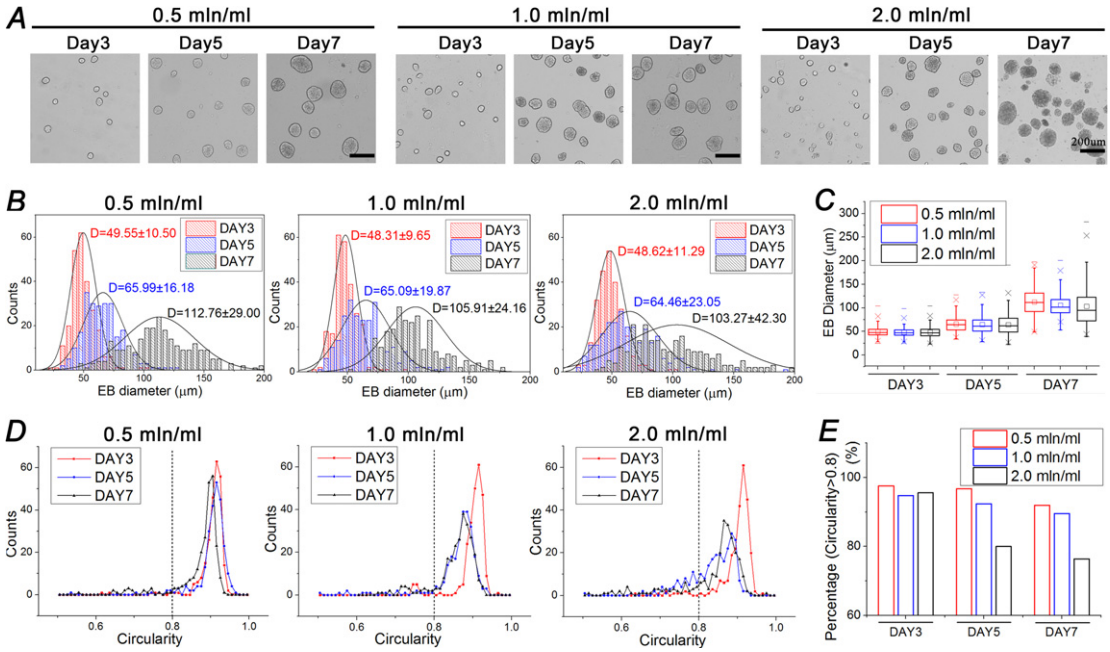

Figure 6. EB formation in different cell density: (A) optical images of released EBs at different days. (B) EB diameter and (C) EB circularity distributions at different days. Summary of the (D) diameter and (E) circularity. 250 EBs were applied for diameter and circularity measurements for each group. Scale bar: 200 μm.

250 random EBs for each sample, the histogram of EB diameter were obtained, showing a Gauss distribution curve (figure 6(B)). The results demonstrated that the EB size increased significantly from about 50 μm to about 110 μm when the construct was cultured from day 3 to day 7 (figure 6(C)). Cell density had little influence on EB average size. However, increased cell density would result in the reduction of the uniformity of EB size, especially at day 7; the EB diameter of 2.0 mln mL^{-1} group at day 7 was vastly heterogeneous, with a deviation of 42.30 μm, which was much more than those of other two groups.

Circularity was measured to assess the quality of EBs (figure 6(D)). For the 0.5 mln mL^{-1} group, most of the EBs were close to a standard spheroid with the circularity centered in 0.9 for the three time points. As to the other two groups, the circularity at day 3 is similar to that of 0.5 mln mL^{-1} group, while the circularity frequency peaks had a significant decrease at day 5 and day 7. In particular, about 20% EBs had a circularity under 0.8 at day 5 and day 7 for the 2.0 mln mL^{-1} group. In general, the circularity decreased with the increase of culture time and initial cell density in the hydrogel (figure 6(E)).

3.6. Comparison with other EB formation methods

Considering this was a novel methodology of EB formation, we systematically compared the commonly used static suspension and hanging drop methods with the 3D bioprinting method for EB formation. As demonstrated by the phase-contrast images (figure 7(A)), EBs generated by static suspension method showed more uncontrollable morphology rather than round spheroid. The distribution of EB diameter clearly demonstrated that 3D bioprinting technology generated EBs with higher uniformity compared with static suspension technology, especially for the larger EB diameter, i.e. 60 $\sim$ 70 μm and 100 $\sim$ 110 μm regions (figure 7(B)). In particular, the EBs with 30 $\sim$ 50 μm diameter presented vastly irregular shape in suspension technology, which was confirmed by the circularity curve (figure 7(C)). On the other hand, EBs generated by 3D bioprinting technology showed higher circularity regardless of the diameter regions, suggesting more regular shape (figure 7(C)). More characteristic like EB forming motivation, size control method, EB diameter range, uniformity, yield, operation complexity were compared among 3D bioprinting technology, static suspension technology and hanging drop technology, as listed in table 1.

4. Discussion

3D cell culture environment and tissue-like models have drawn great attention because they can be tuned to promote certain levels of cell differentiation and tissue organization, which is difficult in traditional 2D culture systems for their failing to reconstitute the *in vivo* cellular microenvironment [30, 31]. Various 3D culture systems have been developed to study the cellular behavior affected by spatial and temporal cell–cell and cell–matrix interactions. Among these methods, 3D bioprinting, typically containing jet-, laser- and extrusion-based methods, is a promising

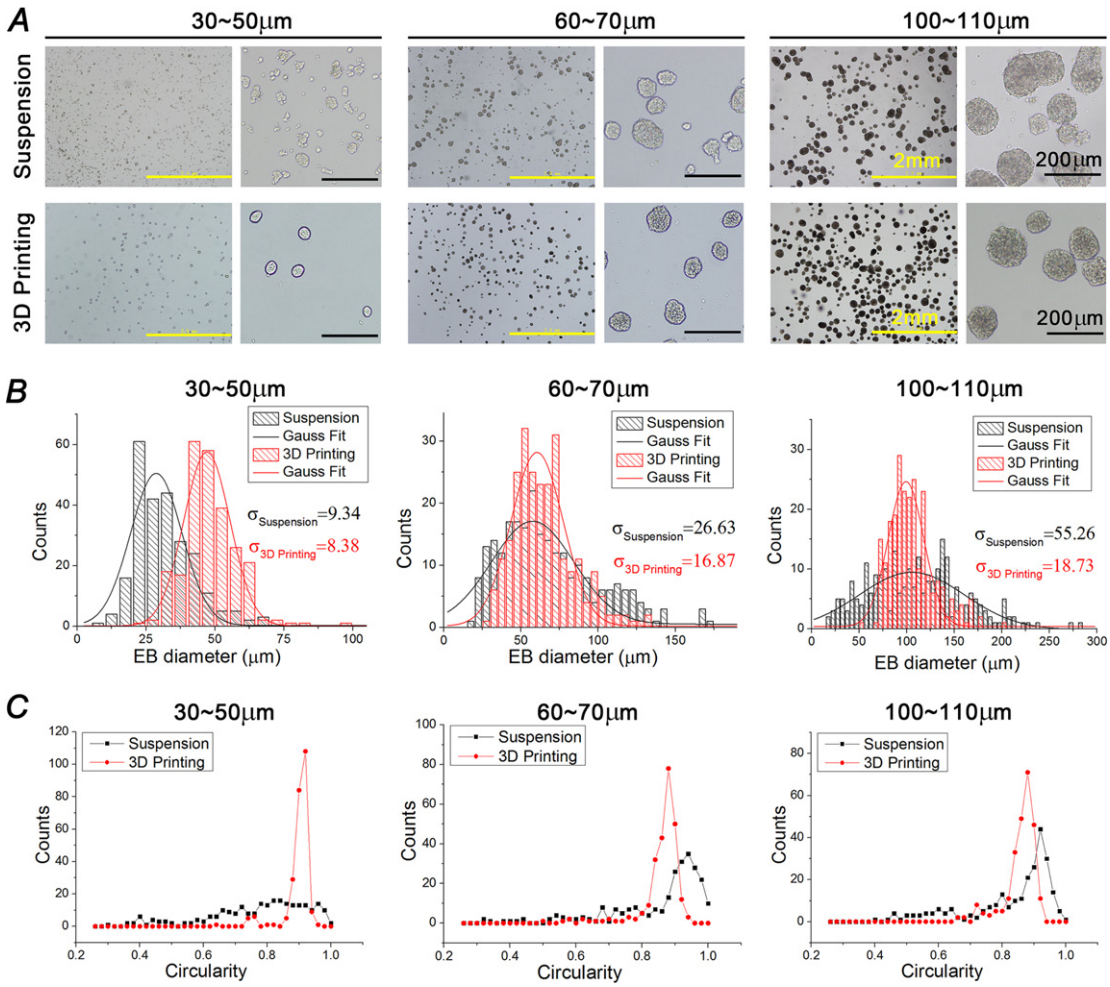

Figure 7. Comparison of static suspension and 3D bioprinting technology for generating EBs. (A) Phase-contrast images showing the morphology of EBs generated by static suspension technology and 3D bioprinting technology. (B) The EB diameter histograms presented the distribution of EB size with a Gauss distribution fitting. (C) The circularity curves contrasted the EB qualities.

Table 1. Comparison of three EB forming methods.

	Hanging-drop	Suspension	3D print
Forming mechanism	Aggregation by gravity	Self-aggregation	Proliferation
Size control	Time and cell density	Time and cell density	Mainly time
Diameter range	50 ∼ 500 μm	50 ∼ 500 μm	30 ∼ 200 μm
Uniformity	High	Low	Medium-high
Yield	Low	High	High
Operation	Time-consuming for seeding and medium refresh	Complex for medium refresh	Time-saving and easy for medium refresh

technique to manipulate cells/matrix deposition and ultimately generate 3D complex tissues or organs. This technique have been used in printing cells derived from adult, embryonic and even tumor tissues for tissue engineering and drug screening applications. With the capacity to expand unlimitedly *in vitro* and differentiate into a variety of therapeutic cell types, ESCs have generated great enthusiasm and are being applied in bioprinting studies until recently. As a relatively sensitive cell type, ESCs might suffer greater problems in a printing process compared with other types of cells. Several studies had been conducted to print ESCs, maintaining their viability and pluripotency [16–19]. Instead of creating 3D tissue-like constructs, these studies were more likely to generate cellular droplet array with precise control of distribution. Here we described the work of establishing a 3D ESC-laden hydrogel construct using extrusion-based bioprinting technology. The results demonstrated high proliferation rate of pluripotent ESCs in the hydrogel construct, and a versatile technology for generating highly uniform and high throughput EBs.

Cell viability after 3D bioprinting and construct formation was determined when evaluating the

limitations of bioprinting ESCs. Cells would be lysed or damaged due to osmotic effects in the solution, heat increase and mechanical stress during printing. In the protocol presented in this work, about 6.86% ± 1.31% cells were dead during the cell/hydrogel solution preparation process before 3D bioprinting (figure 2(B)). We assumed this was caused by cell dissociation process, together with the osmosis and stirring operation of hydrogel materials. In an inkjet printing study, 15% Chinese Hamster Ovary cells were detected dead before printing process [32]. Thermal effects of the ejector reservoir in the inkjet printing process and laser force in laser-based printing would be the cause of cell death, in addition to the impact force when cellular droplets were jetted to a rigid substrate in a very short time. Under a different fabricating strategy, the extrusion-based bioprinter extruded the cell-laden cylinders softly on the substrate and controlled the temperature under 30 °C, without the concerns about the thermal and sharply impacting effects. However, cells would inevitably suffer from shear force when the cell-laden hydrogels were continuously extruded through a limited space in the nozzle. We hypothesized that nozzle size and hydrogel viscosity would influence shear force and hence influence cell viability. The cell viability data of different nozzle sizes, chamber and insulation temperatures supported this hypothesis (figures 3(A) and (B)). In our previous study, more than 90% Hela cells were alive after bioprinting under the parameters of Insu-25 °C/Cham-4 °C and Nozzle-260 μm [23], while the viability of ESCs was only 55.52% ± 2.37% under the same parameter combination. When increasing the insulation and chamber temperature to 30 °C and 10 °C respectively, the viability showed a significant increase to 90%. Taking into the account of cell death before bioprinting, optimized parameters led to only 5% cell death during printing, indicating a broad future applicability of this technique to various cell types ranging from tumor cells to ESCs. Additionally, few dead cells were observed during one-week culture period (figure 3(C)). On the other hand, when the culture period was extended to more than 7 days, more and more ESCs suffered from apoptosis and lysis, possibly due to contact inhabitation and insufficient mass transfer to the center of EB with the increasing of EB size. Therefore, 7 days was chose as the experiment time window for this study.

Apart from cell viability, the maintenance of pluripotency is another essential criterion for ESCs regulation and application. The results of immunofluorescence staining and FACS analysis showed a high expression rate (98%) of stem cell pluripotent markers Oct4 and SSEA1 at day 7 (figure 4), indicating that cells remained undifferentiated state during the whole experimental period. Naturally, it can be inferred that the printing process also had little influence on ESC pluripotency.

In the cell-laden hydrogel culture system, both the cell type and matrix material could influence cell growth. Human mesenchymal stem cells remained alive but did not proliferate when encapsulated in alginate [33, 34]. While human ADSCs could proliferated for a short period of time in alginate hydrogel microspheres but showed significantly higher proliferation rate in gelatin/alginate microspheres [35]. As a widely used hydrogel, alginate has the disadvantages of low cell adhesiveness and poor support for cell proliferation [36]. Adding gelatin would improve the cellular adhesive condition and hence favor cell expansion. In this study, the fabricated multilayered constructs offered a 3D microenvironment surrounded by gelatin/alginate materials for ESCs to adhere, self-renew, and cellular spheroid, termed EB, was generated *in situ* because of cell proliferation. Once EB was formed, the spheroid structure supported expansion of subpopulations with differing proliferation, nutrition and oxygenation status compared with conventional monolayer system. It is reported that the proliferation of mouse ESCs was higher when embedded in fibrin gels versus 2D suspension culture [27]. Similarly, in this study, ESCs in 3D constructs proliferated faster than 2D culture sample when being released from hydrogel to read OD value. This operation was aimed to avoid the influence of interactions between reagent molecular and matrix materials (figure 6 and supplement 3). Additionally, the enlargement of EB diameter, which also reflected ESC proliferation, confirmed this result (figure 6).

Typically stimulated via generation of EBs, ESC differentiation depends on numerous cues throughout the EB environment, including EB size and shape, as well as their uniformities. In general, several characteristics should be concerned for EB formation system, including reproducibility, symmetry, ease of use and scalability [37]. In the traditional EB formation methodology, like suspension and hanging-drop, EBs were created via cell gathering and proliferation. In these methods, it was essential to get a balance between allowing necessary ESC aggregation for EB formation and preventing EB agglomeration for efficient cell growth and differentiation [14]. Static suspension cultures produced a large number of EBs with simple operation, but the size and shape of the resulting EBs were highly uncontrollable and irregular due to the tendency of EBs to agglomerate after initial formation, as shown in figure 7. Hanging-drop method served as a golden tool to generate uniform and reproducible EBs with fully aggregating of cells under gravity and non-agglomeration of EBs in different drops. However, it faced the intrinsic limitation of scalability. The 3D bioprinting method presented in this study addressed some of the problems, producing massively homogeneous EBs with regular shape and controllable shape. In this 3D cell-laden hydrogel system, ESCs were immobilized and restricted to aggregate with each other, and would not agglomerate until they are

large enough to connect with each other. When the initial cell density was increased, the average distance between two original EBs was closer and these EBs are more likely to agglomerate with each other while proliferation, which is also one of the concerns when we choose the experiment time period. As a result, the EB uniformity of 2.0 mln mL^{-1} group was not that good as those of 0.5 mln mL^{-1} and 1.0 mln mL^{-1} groups, especially after culturing for one week (figure 6). Without the initial cell aggregating, the size of EBs in our model was mainly determined by the culture time. Also, it would take longer to reach the same scale of EB diameter compared with suspension method, probably due to the physical constrain of the matrix material. For example, it took 5 days and 2 days to get EBs ranging 60 $\sim$ 70 μm for 3D printing and suspension methods, respectively (figure 7). Besides, thanks to the interconnected channels design in the 3D construct which allowed mass transfer, EBs could be produced in a large scale by changing the construct volume and cell density. In the six-layer construct with 1.0 million cells per milliliter for example, EBs got a stable yield of about 3000 cm^{-2}, while the EB yield by suspension technology was about 900 cm^{-2} (seeding 0.5 million cells in a 35 mm dish) and no more than 10 EBs [38] could be produced in 1 cm^2 area in hanging-drop method, which was also demonstrated by our experiments (supplement 4).

In summary, this study presented the high throughput production of pluripotent, uniform, regular and controllable EBs with the diameter smaller than 150 μm during one week culture. In a gelatin-based laser printing method, EBs with the diameter of about 100 μm were also generated to avoid EB agglomeration in gels [19]. EBs with different size exhibit different gene expression and differentiation fate. Park *et al* [39] found that 100 μm diameter EBs of mouse ESCs expressed increased ectoderm markers while 500 μm diameter EBs expressed endoderm and mesoderm markers. Furthermore, Messana *et al* [12] demonstrated that mouse ESCs derived from small EBs ($<$100 μm) had a greater chondrogenic potential than those from larger EBs. Hwang [10] reported that human endothelial cell differentiation was increased in smaller EBs (150 μm) while cardiogenesis was enhanced in larger EBs (450 μm). However, large EBs might be associated with limited mass transfer and the diffusion of biochemical through EBs is demonstrated to be linked to differentiation of ESCs [40]. While the effect of EB size on differentiation remains to be shown in our model, we hypothesize that EBs with the diameter smaller than 150 μm would mediate specific differentiation trajectory, which will be confirmed in the future work.

Demonstrating the advantages of reproducibility, high throughput, regular shape and controlled size, we believe this is a versatile technology for EB generation. But, this 3D printing system does not serve as an EB formation method solely. The ESC-laden hydrogel 3D construct can be dissolved at a proper time point to harvest massive EBs with desired size for ES cell research. Or, the ESC-laden hydrogel 3D construct can be maintained to perform 3D ESC differentiation studies to explore the regulation of EB size, matrix material and 3D structure on ESC differentiation lineages. Furthermore, this technology hold the potential to serve as a versatile tool for the generation of tissue-like structure and organ/tissue on chip based on controlled ESC differentiation.

5. Conclusion

In this study, we reported successful bioprinting of mouse ESCs with hydrogel into a 3D multilayered construct for the first time. Extrusion-based bioprinting technology was applied. Upon parameter optimization, ESCs demonstrated high viability of 90% after 3D printing and construct formation. Cells continued self-renewal in the construct and exhibited a higher proliferation rate compared with conventional 2D culture. 98% cells expressed the canonical pulripotent markers Oct4 and SSEA1 at day 7, indicating that most of the ESCs remained undifferentiated state after printing and culturing. Large quantities of uniform EBs with regular shape and adjustable size were generated through cell proliferation, while avoiding EBs agglomeration. This work indicated the feasibility of fabricating complex 3D tissue-like model based on pluripotent stem cells for applications in pharmacy, regenerative medicine, stem cell expansion and biology studies.

Acknowledgments

The authors acknowledge the funding supports from the National Natural Science Foundation of China (No. 51235006), the National High Technology Research and Development Program of China-863 Program (No. 2012AA020506), the Independent Scientific Research Program of Tsinghua University (No. 2014z21030) and the Beijing Municipal Science & Technology Commission Key Project (No. Z141100002814003). This work was also supported by the National Natural Science Foundation of China Grant 31171381 and the National Basic Research Program of China, 973 program grant 2012CB966701 to (JN), and the funding of the Tsinghua-Peking Center for Life Sciences.

References

[1] Murry C E and Keller G 2008 Differentiation of embryonic stem cells to clinically relevant populations: lessons from embryonic development *Cell* **132** 661–80

[2] Dang S M, Gerecht-Nir S, Chen J, Itskovitz-Eldor J and Zandstra P W 2004 Controlled, scalable embryonic stem cell differentiation culture *Stem cells* **22** 275–82

[3] Watt F M and Hogan B L M 2000 Out of Eden: stem cells and their niches *Science* **287** 1427–30

[4] Zhang H, Dai S, Bi J and Liu K K 2011 Biomimetic three-dimensional microenvironment for controlling stem cell fate *Interface Focus* **1** 792–803

[5] Guilak F, Cohen D M, Estes B T, Gimble J M, Liedtke W and Chen C S 2009 Control of stem cell fate by physical interactions with the extracellular matrix *Cell Stem Cell* **5** 17–26

[6] Fennema E, Rivron N, Rouwkema J, van Blitterswijk C and de Boer J 2013 Spheroid culture as a tool for creating 3D complex tissues *Trends Biotechnol.* **31** 108–15

[7] Yao R, Wang J Y, Li X K, Jung D J, Qi H, Kee K K and Du Y N 2014 Hepatic differentiation of human embryonic stem cells as microscaled multilayered colonies leading to enhanced homogeneity and maturation *Small* **10** 4311–23

[8] Hurtley S 2009 Location, locaton, location *Science* **326** 1205

[9] Ruiz S A and Chen C S 2008 Emergence of patterned stem cell differentiation within multicellular structures *Stem cells* **26** 2921–7

[10] Hwang Y S, Chung B G, Ortmann D, Hattori N, Moeller H C and Khademhosseini A 2009 Microwell-mediated control of embryoid body size regulates embryonic stem cell fate via differential expression of WNT5a and WNT11 *Proc. Natl Acad. Sci. USA* **106** 16978–83

[11] Mummery C L, Zhang J, Ng E S, Elliott D A, Elefanty A G and Kamp T J 2012 Differentiation of human embryonic stem cells and induced pluripotent stem cells to cardiomyocytes: a methods overview *Circ. Res.* **111** 344–58

[12] Messana J M, Hwang N S, Coburn J, Elisseeff J H and Zhang Z 2008 Size of the embryoid body influences chondrogenesis of mouse embryonic stem cells *J. Tissue Eng. Regenerative Med.* **2** 499–506

[13] Dang S M, Kyba M, Perlingeiro R, Daley G Q and Zandstra P W 2002 Efficiency of embryoid body formation and hematopoietic development from embryonic stem cells in different culture systems *Biotechnol. Bioeng.* **78** 442–53

[14] Rungarunlert S, Techakumphu M, Pirity M K and Dinnyes A 2009 Embryoid body formation from embryonic and induced pluripotent stem cells: benefits of bioreactors *World J. Stem Cells* **1** 11–21

[15] Moeller H C, Mian M K, Shrivastava S, Chung B G and Khademhosseini A 2008 A microwell array system for stem cell culture *Biomaterials* **29** 752–63

[16] Xu F, Sridharan B, Wang S, Gurkan U A, Syverud B and Demirci U 2011 Embryonic stem cell bioprinting for uniform and controlled size embryoid body formation *Biomicrofluidics* **5** 22207

[17] Faulkner-Jones A, Greenhough S, King J A, Gardner J, Courtney A and Shu W 2013 Development of a valve-based cell printer for the formation of human embryonic stem cell spheroid aggregates *Biofabrication* **5** 015013

[18] Raof N A, Schiele N R, Xie Y, Chrisey D B and Corr D T 2011 The maintenance of pluripotency following laser direct-write of mouse embryonic stem cells *Biomaterials* **32** 1802–8

[19] Dias A D, Unser A M, Xie Y, Chrisey D B and Corr D T 2014 Generating size-controlled embryoid bodies using laser direct-write *Biofabrication* **6** 025007

[20] Yan Y *et al* 2005 Fabrication of viable tissue-engineered constructs with 3D cell-assembly technique *Biomaterials* **26** 5864–71

[21] Yao R, Zhang R J, Yan Y N and Wang X H 2009 *In vitro* angiogenesis of 3D tissue engineered adipose tissue *J. Bioact. Compat. Polym.* **24** 5–24

[22] Zhang T, Yan K C, Ouyang L L and Sun W 2013 Mechanical characterization of bioprinted *in vitro* soft tissue models *Biofabrication* **5** 045010

[23] Zhao Y, Yao R, Ouyang L, Ding H, Zhang T, Zhang K, Cheng S and Sun W 2014 Three-dimensional printing of Hela cells for cervical tumor model *in vitro Biofabrication* **6** 035001

[24] Ouyang L, Yao R, Chen X, Na J and Sun W 2015 3D printing of HEK 293FT cell-laden hydrogel into macroporous constructs with high cell viability and normal biological functions *Biofabrication* **7** 015010

[25] Magyar J P, Nemir M, Ehler E, Suter N, Perriard J C and Eppenberger H M 2001 Mass production of embryoid bodies in microbeads *Ann. New York Acad. Sci.* **944** 135–43

[26] Dang S M, Kyba M, Perlingeiro R, Daley G Q and Zandstra P W 2002 Efficiency of embryoid body formation and hematopoietic deelopment from embryonic stem cells in different culture systems *Biotechnol. Bioeng.* **78** 442–53

[27] Liu H, Collins S F and suggs L J 2006 Three-dimensional culture for expansion and differentiaion of mouse embryonic stem cells *Biomaterials* **27** 6004–14

[28] Gerecht S, Burdick J A, Ferreira L S, Townsend S A, Langer R and Vunjak-Novakovic G 2007 Hyaluronic acid hydrogel for controlled self-renewal and differentiation of human embryonic stem cells *Proc. Natl Acad. Sci. USA* **104** 11298–303

[29] Gaetani R, Doevendans P A, Metz C H G, Alblas J, Messina E, Giacomello A and Sluijtera J P G 2012 Cardiac tissue engineering using tissue printing technology and human cardiac progenitor cells *Biomaterials* **33** 1782–90

[30] Huh D, Hamilton G A and Ingber D E 2011 From 3D cell culture to organs-on-chips *Trends Cell Biol.* **21** 745–54

[31] Yao R, Du Y, Zhang R, Lin F and Luan J 2013 A biomimetic physiological model for human adipose tissue by adipocytes and endothelial cell cocultures with spatially controlled distribution *Biomed. Mater.* **8** 045005

[32] Xu T, Jin J, Gregory C, Hickman J J and Boland T 2005 Inkjet printing of viable mammalian cells *Biomaterials* **26** 93–9

[33] Markusen J F, Mason C, Hull D A, Town M A, Tabor A B, Clements M, Boshoff C H and Dunnill P 2006 Behavior of adult human mesenchymal stem cells entrapped in alginate-GRGDY beads *Tissue Eng.* **12** 821–30

[34] Tang M, Chen W, Weir M D, Thein-Han W and Xu H H 2012 Human embryonic stem cell encapsulation in alginate microbeads in macroporous calcium phosphate cement for bone tissue engineering *Acta Biomater.* **8** 3436–45

[35] Yao R, Zhang R, Luan J and Lin F 2012 Alginate and alginate/gelatin microspheres for human adipose-derived stem cell encapsulation and differentiation *Biofabrication* **4** 025007

[36] Yao R, Zhang R, Lin F and Luan J 2013 Biomimetic injectable HUVEC-adipocytes/collagen/alginate microsphere co-cultures for adipose tissue engineering *Biotechnol. Bioeng.* **110** 1430–43

[37] Ungrin M D, Joshi C, Nica A, Bauwens C and Zandstra P W 2008 Reproducible, ultra high-throughput formation of multicellular organization from single cell suspension-derived human embryonic stem cell aggregates *PLoS One* **3** e1565

[38] Kurosawa H 2007 Methods for inducing embryoid body formation: *in vitro* differentiation system of embryonic stem cells *J Biosci Bioeng.* **103** 389–98

[39] Park J, Cho C H, Parashurama N, Li Y, Berthiaume F, Toner M, Tilles A W and Yarmush M L 2007 Microfabrication-based modulation of embryonic stem cell differentiation *Lab Chip* **7** 1018–28

[40] Van Winkle A P, Gates I D and Kallos M S 2012 Mass transfer limitations in embryoid bodies during human embryonic stem cell differentiation *Cells Tissues Organs* **196** 34–47